Influence of an insulating megaregolith on heat flow and crustal temperature structure of Mercury

Isabel Egea-González [a,*], Javier Ruiz [b]

[a] Instituto de Astrofísica de Andalucía, CSIC, Glorieta de la Astronomía s/n, 18008 Granada, Spain

[b] Departamento de Geodinámica, Facultad de Ciencias Geológicas, Universidad Complutense de Madrid, 28040 Madrid, Spain

* Corresponding author. E-mail: isaegea@iaa.es (I. Egea-González).

Tel:+34958121566 Fax: +34958814530

Abstract

Mercury is covered by a megaregolith layer, which constitutes a poor thermally conducting layer that must have an influence on the thermal state and evolution of the planet, although most thermal modeling or heat flow studies have overlooked it. In this work we have calculated surface heat flows and subsurface temperatures from the depth of thrust faults associated with several prominent lobate scarps on Mercury, valid for the time of the formation of these scarps, by solving the heat equation and taking into account the insulating effects of a megaregolith layer. We conclude that megaregolith insulation could have been an important factor limiting heat loss and therefore interior cooling and contraction of Mercury. As Mercurian megaregolith properties are not very well known, we also analyze the influence of these properties on the results, and discuss the consequences of imposing the condition that the total radioactive heat production must be lower than the total surface heat loss (this is, the Urey ratio, *Ur*, must be lower than 1) in a cooling and thermally contracting planet such as Mercury at the time of scarp emplacement. Our results show that satisfying the condition of $Ur < 1$ implies that the average abundances of heat-producing elements silicate layer is 0.4 times or less the average surface value, placing an upper bound on the bulk content of heat producing elements in Mercury's interior.

Key words: Mercury; Regoliths; Thermal histories.

1. Introduction

In Mercury, as in other bodies that lack a substantial atmosphere, impact processes may have resulted in the production of a megaregolith layer, which is a porous, fragmentary layer formed by large compact and coherent blocks with regolith

material filling the gaps between them. This rubble has impact and ejecta origin, and covers the outer few meters-kilometers of a planet (e.g., Warren and Rasmussen, 1987; Ziethe et al., 2009). Because megaregolith has a thermal conductivity much lower than that of equivalent solid rock, it insulates the hot interior and slows down cooling. Therefore, megaregolith has an influence on the thermal state and evolution of the planet.

Previous works have estimated paleo-heat flows for Mercury from the depth of large thrust faults associated with lobate scarps, interpreted to reach the crustal brittle-ductile transition (BDT) depth (Watters et al., 2002; Nimmo and Watters, 2004; Egea-Gonzalez et al., 2012), or from the effective elastic thickness of the lithosphere (Ruiz et al., 2013); the so-obtained paleo-heat flow values refer to the time of deformation (i.e., the time of faulting or loading). Works calculating heat flows from proxies of lithospheric strength relate the mechanical state of the lithosphere to their thermal structure through procedures which involve the surface temperature. These works disregard the effects of an insulating megaregolith, although such a thermally insulating blanket would reduce the interior heat loss, which in turn would imply lower surface heat flows derived from the BDT depth (Ruiz and Tejero, 2000), the raising of near-surface crustal temperatures and the reduction of thermal gradients below the megaregolith.

Another way to analyze the thermal evolution of Mercury is through thermal history models (e.g., Hauck et al., 2004; Grott et al., 2011; Williams et al., 2011; Tosi et al., 2013). Most of them neglect the presence of a megaregolith layer, resulting in enhanced heat dissipation, and hence in substantial planetary cooling and contraction, which is hard to reconcile with the relatively limited observed global contraction deduced from shortening measurements in compressional structures (for an updated

77 estimate of radial contraction see Watters et al. 2013). On the other hand, Grott et al.
78 (2011) demonstrated that the inclusion of an insulating megaregolith layer has important
79 implications on the thermal evolution of Mercury, since predicted planetary cooling and
80 radial contraction are notably reduced, relaxing the severe constraints imposed by the
81 observed contraction.
82 In this work, we consider the effect of an insulating megaregolith layer in the
83 calculation of surface heat flow and crustal thermal structure from the depth of thrust
84 faults associated with several prominent lobate scarps on Mercury. We first derive
85 upper limits for the surface heat flow by neglecting the megaregolith layer. Then, we
86 solve the heat equation by taking into account the properties of a typical Lunar
87 megaregolith, in accordance with previous studies which considered the Lunar
88 megaregolith as a good analog for Mercury (Grott et al., 2011). Furthermore, as
89 Mercurian megaregolith properties are not very well known, we also analyze the
90 influence on the results of higher thermal conductivities, and the implications of the
91 condition that the heat loss through the surface must be higher than the heat generated
92 internally by radioactive decay in a cooling planet.
93
94 **2. Study areas**
95 Lobate scarps are the most prominent tectonic features on Mercury, and are
96 interpreted to be the surface expressions of thrust faults related to global thermal
97 contraction of the planet (e.g., Strom et al., 1975; Watters et al., 2009). In this work we
98 have calculated surface heat flows for three different regions of Mercury by using
99 published values of the BDT depth estimated from the analysis of thrust faults
100 associated with lobate scarps (coordinates for the studied lobate scarps are given in
101 **Table 1**). Watters et al. (2002) used a mechanical dislocation model to obtain a BDT

depth of 35-40 km beneath the Discovery Rupes lobate scarp (hereafter Region A). Ritzer at al. (2010) employed a similar method to analyze the geometries of two faults associated with two lobate scarps located at the equator (Region B), and they obtained a BDT depth of 35 km for both structures. Egea-Gonzalez et al. (2012) studied the depth of faulting for three lobate scarps located in the Kuiper region of Mercury (Region C); the depth of faulting estimated by these authors ranges from 30 to 39 km.

3. Temperature at the brittle-ductile transition.

In order to obtain surface heat flows, we solve the heat equation. To establish the integration constants that are involved in this calculation, we take into account the temperature at the brittle-ductile transition (T_{BDT}) and the surface temperature (T_S). As the brittle strength is a function of depth and the ductile strength depends on temperature, we can equate both strength expressions at the brittle-ductile transition with the purpose of working out the value of the temperature at the BDT depth.

Smith et al. (2012) have shown that there are large variations in crustal thickness on Mercury. Our studied regions have crustal thicknesses ranging from similar (Region B) to clearly higher (Region C) than the mean value of 50 km assumed by these authors. For these regions, the crustal thicknesses values in Smith et al. (2012) are certainly thicker than the local BDT depth. Although there are some uncertainties in the absolute values of the crustal thickness model, local variations in this kind of models are robust. Thus we only consider the possibility of a BDT depth in the crust and restrict our calculations to crustal mechanical and thermal properties.

The critical stress difference necessary to cause faulting is given by (e.g., Ranalli, 1997):

$$(\sigma_1 - \sigma_3)_b = \alpha \rho g z, \quad (1)$$

where ρ is the density, g is the acceleration due to the gravity (3.7 m s^{-2}), z is the depth and α is a coefficient that depends on the friction coefficient and on the tectonic regime (α = 3 for thrust faulting). In this expression we have assumed zero pore pressure, which is appropriated for the Mercurian crust. In the lithosphere, ductile deformation takes place mainly by dislocation creep. In such a case the ductile strength is (e.g., Turcotte and Schubert, 2002);

$$(\sigma_1 - \sigma_3)_d = \left(\frac{\dot{\varepsilon}}{A}\right)^{\frac{1}{n}} Exp\left(\frac{Q}{nRT}\right), \quad (2)$$

where $\dot{\varepsilon}$ is the strain rate, A and n are laboratory-determined constants, Q is the activation energy of creep, R is the gas constant (8.31 J mol^{-1} K^{-1}) , and T is the absolute temperature. The brittle and ductile strengths are equal at z_{BDT}, so we can find the value of T_{BDT}:

$$T_{BDT} = \frac{Q}{nR\ \mathrm{Ln}\left[3\rho g z_{BDT}\left(\frac{\dot{\epsilon}}{A}\right)^{-\frac{1}{n}}\right]} \quad (3)$$

This expression can be adapted to consider two different layers in case that megaregolith is assumed:

$$T_{BDT} = \frac{Q}{nR\ \mathrm{Ln}\left[3[\rho_1 z_1 + \rho_2 (z_{BDT} - z_1)] g\left(\frac{\dot{\epsilon}}{A}\right)^{-\frac{1}{n}}\right]} \quad (4)$$

We have used subscript 1 to refer to the megaregolith layer and subscript 2 to apply to the deeper layer. z_1 is the megaregolith thickness.

At the surface we assume temperature values provided by the present-day surface temperature model of Vasavada et al. (1999), which takes into account the insolation dependence on latitude and longitude. **Table 1** shows temperatures on the surface that are representative for the location of the three regions studied here (see also Williams et al. (2011) and Egea-González et al. (2012)).

4. The case without insulating megaregolith

For the case without a megaregolith layer, surface heat flows can be easily calculated by solving the steady-state, 1-D heat conduction equation with radiogenic heat production for a layer of z_{BDT} thickness. We have assumed that thermal conductivity, density, heat capacity and volumetric heat production rate are constant values that represent the average properties of the crust, so the surface heat flow is expressed as:

$$F_S = \frac{k(T_{BDT} - T_S)}{z_{BDT}} + \frac{z_{BDT} H}{2}, \quad (5)$$

where k is the thermal conductivity of the crust and H is the volumetric heat production rate. We use a thermal conductivity of 2 W m^{-1} K^{-1}, a value appropriate for basaltic rocks and for a wide variety of Earth crustal rocks at temperatures of several hundreds of degrees centigrade (e.g., Beardsmore and Cull, 2001).

In order to calculate T_{BDT}, we use crustal properties compatible with MESSENGER data pointing to a dense crust formed mainly through extensive volcanism (Head et al., 2008; Denevi et al., 2009; Nittler et al., 2011; Smith et al.,

2012): a crustal density of 3100 kg m^{-3} and creep parameters for dry Maryland diabase (n = 4.7, Q = 485 kJ mol^{-1} and A = 8 $MPa^{-4.7}s^{-1}$ (Mackwell et al., 1998)). Strain rates used are 10^{-16} s^{-1} - 10^{-19} s^{-1}, where the former value is a characteristic value for active terrestrial plate interiors (e.g., Tesauro et al., 2007), and the latter is a typical value for thermal contraction on terrestrial planets (e.g., Schubert et al., 1988). The obtained T_{BDT} values are shown in **Table 1**; note that higher z_{BDT} values result in lower T_{BDT} values.

In order to calculate volumetric heat production rates, we have taken into account a period of time (t) between 3.2 and 4 Ga, and the average surface abundances of radioactive elements obtained by Peplowsky et al. (2012, 2011) as representative for the entire crust, which give (1.0 - 3.3) × 10^{-4} mW m^{-3}. We assume homogeneously distributed crustal heat sources, because the heavily cratered surface suggests a heavy mixing of the crust (see, for example, the arguments given by Taylor et al. 2006 for the case of Mars). Relevant parameters and obtained surface heat flows are summarized in **Table 1**.

Figure 1 shows the temperature profiles for extreme values of z_{BDT}, t and $\dot{\varepsilon}$ in the case of Region C. Profiles obtained in Regions A and B are similar and are not shown. The calculated heat flows are consistent with results of previous works (Watters et al., 2002; Nimmo and Watters, 2004; Egea-Gonzalez et al., 2012; Ruiz et al., 2013); higher surface heat flows are obtained for shallower z_{BDT} and higher strain rates and volumetric heat production rates.

5. The case with a megaregolith layer.

In this section we solve the 1-D heat conduction equation by including a megaregolith layer in order to analyze its influence on surface heat flows and crustal temperatures above the BDT depth. We assume two layers that are described by

different average parameters and obtain the following expressions:

$$F_S = k_1 a \tag{6}$$

$$T(z) = -\frac{H_1}{2k_1} z^2 + az + T_S\,,\ 0 \le z \le z_1 \tag{7}$$

$$T(z) = -\frac{H_2}{2k_2} z^2 + bz + c,\ z_1 < z \le z_{BDT} \tag{8}$$

where

$$a = \frac{H_2 k_1 (z_{BDT} - z_1)^2 + H_1 k_2 z_1^2 + 2k_1[(T_{BDT} - T_S)k_2 + H_1(z_{BDT} - z_1)z_1]}{2k_1[k_1(z_{BDT} - z_1) + k_2 z_1]}$$

$$b = \frac{k_2[2(T_{BDT} - T_S)k_1 - H_1 z_1^2] + H_2(2k_2 z_1^2 + k_1({z_{BDT}}^2 - z_1^2))}{2k_2(k_1(z_{BDT} - z_1) + k_2 z_1)}$$

$$c = \frac{k_2 z_1[2T_{BDT}k_2 + z_{BDT}H_2(z_{BDT} - 2z_1) + z_{BDT}H_1 z_1]}{2k_2[k_1(z_{BDT} - z_1) + k_2 z_1]} + \frac{k_1[\, z_{BDT}H_2 z_1(-z_{BDT} + z_1) + 2k_2(T_S z_{BDT} - T_{BDT} z_1)]}{2k_2[k_1(z_{BDT} - z_1) + k_2 z_1]}$$

As previously mentioned, subscript 1 refers to the shallower, fractured megaregolith layer and subscript 2 applies to the deeper, consolidated layer. Units of *a* and *b* are K m^{-1}, and c is in K. The deeper layer is characterized by parameters already considered in the previous section: k_2 = 2 W m^{-1} K^{-1}, ρ_2 = 3100 kg m^{-3} and H_2 = (1.0 – 3.3) × 10^{-4} mW m^{-3}.

With regard to the megaregolith layer, as the Moon and Mercury have both heavily cratered surfaces and the greater gravity of Mercury could offset the greater velocity of impactors there, previous studies consider that Lunar and Mercurian megaregoliths could be similar (Grott et al., 2011). We have selected k_1 = 0.2 W m^{-1} K^{-1}, from the relationship between porosity and thermal conductivity derived for the Moon by Warren and Rasmussen (1987). We assume a megaregolith thickness (z_1) of 1 – 5 km. A thickness shallower than 1 km is not expected due to the high velocity of impactors on Mercury, and a blanket deeper than 5 km is unlikely because of the high gravity (Grott et al., 2011). A megaregolith density of 2000 kg m^{-3} has been adopted (see Caarier et al., 1991; Vasavada et al., 2012; Wieczorek et al., 2013). This ρ_1 value supposes that H_1 ranges between (0.6 – 2.1) × 10^{-4} mW m^{-3}. The used properties are listed in **Table 2**.

F_S values obtained from the heat equation solution are shown in **Table 3**. Highest results are related to a thin megaregolith layer, a shallow brittle-ductile transition depth and high values of strain rate and volumetric heat production rate. **Figure 2** displays temperature profiles obtained in Region C from z_{BDT} = 39 km. Thick megaregolith layers, shallow brittle-ductile transition depths and high volumetric heat production rates and strain rates imply hotter temperature profiles above the BDT depth. Comparisions of these results with those obtained in **Section 4** show that an insulating megaregolith reduces surface heat flows and raises temperatures in regions shallower than z_{BDT} notably.

Although previous works concluded that the thermal properties of the megaregolith are similar on Mercury and the Moon, Mercurian megaregolith properties are not very well known. Differences in temperatures and geologic activity, with persistent volcanism on Mercury, could lead to differences in fractures, porosities and

thermal conductivities between the Moon and Mercury megaregoliths. Thus, we have performed calculations in order to illustrate the influence of different thermal conductivities on surface heat flows and subsurface temperatures.

Figure 3 displays the highest F_S values in Region C as a function of k_1. This figure shows that the surface heat flow increases, whereas crustal temperatures above z_{BDT} decrease, with megaregolith thermal conductivity. Thus, the cases withouth megaregolith considered in the previous section represent upper limits for the paleo-heat flows derived from the BDT depth, and conversely represent lower limits for crustal temperatures above z_{BDT}. Variations in the results due to differences in megaregolith density are negligible because of the weak dependence of surface heat flows and crustal temperature on this property.

6. Discussion and conclusions.

Our results clearly demonstrate that an insulating megaregolith layer notably influences the thermal state of Mercury, through increasing subsurface temperatures and reducing surface heat flows. Heat flows derived in **Section 4** must be considered as upper limits for Mercury, because the effect of the megaregolith was not taken into account there, while crustal temperatures above z_{BDT} are lower limits for each studied region. Lower surface heat flows are obtained by taking into account a Lunar-like megaregolith. The upper range of values is in agreement with results obtained by Grott et el. (2011). The lower range in surface heat flows that we have obtained is difficult to reconcile with the planetary cooling required to originate global contraction and lobate scarps (see Ruiz et al., 2013). With respect to temperatures, hotter temperature profiles are related to thicker megaregolith layers, lower strain rates and higher volumetric heat production rates. Several extreme combinations of parameters involving highest z_{BDT}

values, thicker megaregolith layers, and higher volumetric heat production rates lead to a maximum in temperature profiles implying a negative heat flow. This excludes such combinations of parameters.

Figure 4 shows surface heat flows as a function of thermal conductivity and thickness of the megaregolith, for strain rates and z_{BDT} maximizing heat flow. H has been calculated from the mean values provided by Peplowski et al. (2011, 2012). It is interesting to note that the upper range of obtained heat flows is compatible with those reported by Grott et al. (2011) in their nominal thermal history model.

The heat flow and the actual megaregolith influence may potentially be constrained by the condition that the total radioactive heat production must be lower than the total surface heat loss in a cooling and thermally contracting planet (Ruiz et al., 2013); the Urey ratio (Ur) is the ratio between the total heat production and the total heat loss, and must be lower than 1 for interior planetary cooling. The radioactive heat production can be expressed as an equivalent surface heat flow, and **Figure 4** also shows upper and lower limits for the radioactive component of heat flow, calculated considering that the silicate portion of the planet is a spherical shell with outer radius of 2440 km, and mean density and thickness of, respectively, 3380 kg m^{-3} and 420 km (Hauck et al., 2013). The radioactive elements abundances are based on the mean MESSENGER values (Peplowski et al., 2011, 2012), but taking into account that mantle abundances must be lower than surface abundances, because the high incompatibility of these elements concentrates them in the crust; we consider the cases with bulk radioactive elements abundances in the silicate layer of 0.2, 0.3 and 0.4 times the average surface value. Our results show that satisfying the condition of $Ur < 1$ is favored by a thinner megaregolith layer, a higher thermal conductivity of the megaregolith, an average radioactive element abundance in the silicate fraction

293 substantially lower than the surface value, or some combination of these possibilities.
294 Most importantly, our results indicate that average abundances of heat-producing
295 elements in the silicate layer is 0.4 times or less the average surface value, which is in
296 agreement with results obtained by Ruiz et al. (2013). This result is robust, since it
297 holds irrespective of the assumed thermal conductivities and densities, and serves to
298 place an upper bound on the bulk content of heat producing elements in Mercury's
299 interior.

300 The crust of Mercury is considered to be mostly basaltic, although ultra-mafic
301 rocks could be present (Nittler et al., 2011). Ultra-mafic rocks have generally thermal
302 conductivities higher (e.g., Clauser and Huenges, 1995) than our nominal value of 2 W
303 m^{-1} K^{-1}, which is appropriate for rocks of basaltic composition. A higher crustal thermal
304 conductivity would involve higher surface heat flows. If for example a crustal thermal
305 conductivity of 2.5 W m^{-1} K^{-1} is considered, then the obtained surface heat flow ranges
306 would be 21-38 mW m^{-2} and 9-29 mW m^{-2} for the cases without and with megaregolith,
307 respectively. For the cases without megaregolith, crustal temperatures above the BDT
308 depth would be lower than those obtained in **Section 4**, whereas in cases including
309 megaregolith the derived temperature profiles are, in general, similar to those obtained
310 in **Section 5**. Thus, the effect of using a higher crustal thermal conductivity is not very
311 important for our evaluation of the insulating effects of a megaregolith layer.

312 Our results clearly evidence that an improved knowledge of the properties of the
313 megaregolith is necessary for addressing key questions on the Mercurian nature and
314 evolution. Megaregolith insulation could indeed have been an important factor limiting
315 heat loss and therefore interior cooling through the history of Mercury. It could help to
316 explain the limited contraction observed. In any case, the insulating effect of the
317 megaregolith cannot have been sufficiently high for precluding the contraction of this

318 planet, at least for the time when most of large lobate scarps were originated. Thus,
319 further research on contraction history and megaregolith properties is fundamental for
320 our understanding of the thermal and internal evolution, as well as the present-day state,
321 of Mercury.
322
323 **Acknowledgements**
324 We thank the comments and suggestions from two anonymous reviewers. IEG is
325 thankful to the Spanish MINECO. JR work was supported by a contract Ramón y Cajal
326 co-financed from the Ministerio de Economía y Competitividad of Spain and the
327 European Social Fund (ESF).
328
329 **References**
330 Aharonson, O., Zuber, M. T., Solomon, S. C., 2004. Crustal remanence in an internally
331 magnetized non-uniform shell: a possible source for Mercury's magnetic field?
332 *Earth and Planet. Sci. Lett*., 218, 261–268.
333 Beardsmore, G.R. and Cull, J.P., 2001. Crustal heat flow. A guide to measurement and
334 modelling, Cambridge Univ. Press, Cambridge, 324 pp.
335 Carrier, W.D., Olhoeft, G.R. and Mendell, W., 1991. Lunar Sourcebook, cap. Physical
336 Properties of the Lunar Surface. Cambridge University Press, Cambridge.
337 Carslaw, H.S. and Jaeger, J.C., 1959. Conduction of heat in solids. (2nd Edit.). Oxford
338 University Press, London.
339 Chase, S.C., Miner, E.D., Morrison, D. et al., 1974. Preliminary infrared radiometry of
340 the night side of Mercury from Mariner 10. *Science*, 185, 142–145.
341 Chase, S. C., Jr., Miner, E. D., Morrison, D. et al., 1976. Mariner 10 infrared radiometer
342 results - Temperatures and thermal properties of the surface of Mercury. *Icarus.*

28, 565-578.

Clauser, C. and Huenges, E., 1995. Thermal Conductivity of Rocks and Minerals. In: T. J. Ahrens (ed), Rock Physics and Phase Relations - a Handbook of Physical Constants, AGU Reference Shelf, Vol. 3, pp. 105-126, American Geophysical Union, Washington.

Cuzzi, J. N., 1974. The Nature of the Subsurface of Mercury from Microwave Observations at Several Wavelengths. *ApJ*., 189, 577-586.

Denevi, B.W., Robinson, M.S., Solomon, S.C. et al., 2009. The Evolution of Mercury's Crust: A Global Perspective from MESSENGER. *Science*, 324, 613-618.

Di Achille, G., Popa, C., Massironi, M. et al., 2012. Mercury's radius change estimates revisited using MESSENGER data. *Icarus*, 221, 456-460.

Domingue, D.L., Vilas, F., Holsclaw, G. M. et al., 2010. Whole-disk spectrophotometric properties of Mercury: Synthesis of MESSENGER and ground-based observations. *Icarus*, 209, 101–124.

Domingue, D. L., Murchie, S. L., Chabot, N. L. et al., 2011. Mercury's spectrophotometric properties: Update from the Mercury Dual Imaging System observations during the third MESSENGER flyby. Planet. Spa. Sci., 59, 1853-1872.

Egea-González, I., Ruiz, J., Fernández, C. et al., 2012. Depth of faulting and ancient heat flows in the Kuiper region of Mercury from lobate scarp topography. *Planet. Spa. Sci.*, 60, 193-198.

Grott, M., Breuer, D., Laneuville, M., 2011. Thermo-chemical evolution and global contraction of Mercury. *Earth and Planet. Sci. Lett.*, 307, 135–146.

Hapke, B., Danielson, G.E., Klaasen, K. et al., 1975. Photometric observations of Mercury from Mariner 10. *J. Geophys. Res.*, 80, 2431–2443.

368 Hauck, S.A., Dombard, A.J., Phillips, R.J., Solomon, S.C., 2004. Internal and tectonic
369 evolution of Mercury. *Earth and Planet. Sci. Lett*., 222, 713-728.
370 Hauck, Steven A., Margot, Jean-Luc, Solomon, Sean C. et al., 2013. The curious case of
371 Mercury's internal structure. *J. Geophys. Res.*, 118, 6, 1204-1220.
372 Head, J.W., Murchie, S.L., Prockter, L.M. et al., 2008. Volcanism on Mercury:
373 Evidence from the First MESSENGER Flyby. *Science*, 321, 69-72.
374 Head, J. W., Chapman, C. R.; Strom, R. G. et al., 2011. Flood Volcanism in the
375 Northern High Latitudes of Mercury Revealed by MESSENGER. *Science*, 333,
376 1853.
377 Kiselev, N.N. and Lupishko, D.F., 2004. Properties and Peculiarities of Mercury's
378 Regolith disk-integrated Polarimetry in 2000-2002. *Solar System Research*, 38,
379 85–92.
380 Mitchell, D. L., de Pater, I., 1994. Microwave imaging of Mercury's thermal emission at
381 wavelengths from 0.3 to 20.5 CM. *Icarus*, 110, 2-32.
382 Mackwell, S.J., Zimmerman, M.E., Kohlstedt, D.L., 1998. High-temperature
383 deformation of dry diabase with application to tectonics on Venus. *J. Geophys.*
384 *Res.*, 103, 975-984.
385 Morrison, D., 1970. Thermophysics of the planet Mercury. *Space Sci. Rev.*, 11, 271-
386 307.
387 Nimmo, F. and Watters, T.R., 2004. Depth of faulting on Mercury: implications for heat
388 flux and crustal and effective elastic thickness. *Geophys. Res. Lett*., 31, L02701,
389 doi:10.1029/2003GL018847.
390 Nittler, L.R., Starr, S.Z., Weider R.D. et al., 2011. The Major-Element Composition of
391 Mercury's Surface from MESSENGER X-ray Spectrometry. *Science*, 333, 1847.
392 Peplowski, P. N., Lawrence, D. J., Rhodes, E. A., et al. 2012. Variations in the

393 abundances of potassium and thorium on the surface of Mercury: Results from the
394 MESSENGER Gamma-Ray Spectrometer. *J. Geophys. Res.*, 117, E00L04,
395 doi:10.1029/2012JE004141.
396 Ranalli, G., 1997. Rheology of the lithosphere in space and time. *Geol. Soc. Spec. Pub.*,
397 121, 19-37.
398 Ritzer, J.A., Hauck, S.A., Barnouin, O.S. et al., 2010. Mechanical Structure of
399 Mercury's Lithosphere from MESSENGER Observations of Lobate Scarps. *Lunar*
400 *Planet. Sci. Conf. 41st.*, Abstract 1533.
401 Ruiz, J., Tejero, R., 2000. Heat flows through the ice lithosphere of Europa. *J. Geophys.*
402 *Res.*, 105, E12, 29283-29290.
403 Ruiz, J., López, V., Egea-González, I., 2013. Paleo-heat flows, radioactive heat
404 generation, and the cooling and deformation history of Mercury. *Icarus*, in press.
405 Schubert, G., Ross, M. N., Stevenson, D. J., Spohn, T., 1988. Mercury's thermal history
406 and the generation of its magnetic field. Mercury, edited by F. Vilas, C.R.
407 Chapman, and M.S. Matthews, 429-460. Univ. of Arizona Press, Tucson.
408 Smith, D.E., Zuber, M.T., Phillips, R.J. et al. 2012. Gravity field and internal structure
409 of Mercury from MESSENGER. *Science*, 336, 214-217.
410 Strom, R. G., Trask, N. J., Guest, J. E., 1975. Tectonism and volcanism on Mercury. *J.*
411 *Geophys. Res.*, 80, 2478-2507.
412 Taylor, G.J., Boynton, W., Brückner, J. et al., 2006. Bulk composition and early
413 differentiation of Mars. *J. Geophys. Res.*, 111, E03S10.
414 Tesauro, M, Kaban, M. K., Cloetingh, S. A. et al., 2007. 3D strength and gravity
415 anomalies of the European lithosphere. *Earth and Planet. Sci. Lett.*, 263, 56-73.
416 Tosi, N., Grott, M, Plesa, A.-C. et al., Thermo-chemical evolution of Mercury's interior.
417 *J. Geophys. Res.*, doi: 10.1002/jgre.20168, in press.

418 Turcotte, D.L., Schubert, G., 2002. Geodynamics. Cambridge Univ. Press, Cambridge.
419 van Hemelrijck, E. and Vercheval, J., 1981. Some aspects of the solar radiation incident
420 at the top of the atmospheres of Mercury and Venus. *Icarus*, 48, 167–179.
421 Vasavada, A. R., Paige, D. A., Wood, S. E., 1999. Near-surface temperatures on
422 Mercury and the Moon and the stability of polar ice deposits. *Icarus*, 141, 179-
423 193.
424 Vasavada, A. R., Bandfield, J. L., Greenhagen, B. T. et al., 2012. Lunar equatorial
425 surface temperatures and regolith properties from the Diviner Lunar Radiometer
426 Experiment. *J. Geophys. Res.*, 117, E00H18.
427 Warell, J., 2004. Properties of the Hermean regolith IV: photometric parameters of
428 Mercury and the Moon contrasted with Hapke modelling. *Icarus*, 167, 271–286.
429 Warren, P.H. and Rasmussen, K.L., 1987. Megaregolith insulation, internal
430 temperatures, and bulk uranium content of the Moon. *J. Geophys. Res.*, 92, 3453-
431 3465.
432 Watters, T.R., Schultz, R.A., Robinson, M.S. et al., 2002. The mechanical and thermal
433 structure of Mercury´s early lithosphere. *Geophys. Res. Lett.*, 29,
434 10.1029/2001GL014308.
435 Watters, T.R., Solomon, S.C., Robinson, M.S. et al., 2009. The tectonics of Mercury:
436 The view after MESSENGER's first flyby. Earth and Planet. Sci. Lett. 285, 283-
437 296.
438 Watters, T. R., Solomon, S. C., Klimczak, C. et al., 2013. Distribution of prominent
439 lobate scarps on Mercury: contribution to global radial contraction. Lunar Planet.
440 Sci. Conf. 44st. Abstract 2213.
441 Whittington, A. G., Hofmeister, A. M., Nabelek, P. I., 2009. Temperature-dependent
442 thermal diffusivity of the Earth's crust and implications for magmatism. *Nature*,

458, 319-321.

Wieczorek, M. A., Nimmo, F., Kiefer, W. S. et al., 2013. High-Resolution Estimates of Lunar Crustal Density and Porosity from the GRAIL Extended Mission. *Lunar Planet. Sci. Conf. 44th*., Abstract 1719, p.1914.

Williams, J.P., Ruiz, J., Rosenburg, M.A., et al., 2011. Solar insolation driven variations of Mercury's lithospheric strength. *J. Geophys. Res*., 116, E01008, doi: 10.1029/2010JE003655.

Ziethe, R., Seiferlin, K., Hiesinger, H., 2009. Duration and extent of lunar volcanism: Comparison of 3D convection models to mare basalt ages. *Planet. Space Sci.*, 57, 784-796.

Figure Captions

Table 1. Relevant parameters and surface heat flows calculated by neglecting the megaregolith layer. Surface temperature depends on both latitude and longitude due to the coupled spin-orbit resonance and the relatively high eccentricity (Vasavada et al., 1999; Williams et al., 2011).

Figure 1. Temperature profiles in Region C for extreme values of z_{BDT}, t and $\dot{\varepsilon}$ by neglecting megaregolith properties.

Table 2. Properties assumed in our calculations. Subscript 1 refers to the megaregolith layer and subscript 2 refers to properties of the deeper layer.

Table 3. Relevant parameters and extreme surface heat flows calculated by including megaregolith.

Figure 2. Temperature profiles calculated in Region C from z_{BDT} = 39 km and extreme values of z_1, t and $\dot{\varepsilon}$.

Figure 3. Surface heat flows as a function of k_1 in Region C. F_S has been

468 calculated from z_1 = 1, z_{BDT} = 30 km, $\dot{\varepsilon} = 10^{-16}$ $s^{-1}$and $H_1 = 2.1 \times 10^{-4}$ mW m^{-3}.

469 **Figure 4.** Highest surface heat flows in Region C as a function of z_1 for different
470 values of k_1. Dashed black lines represent equivalent radioactive heat flows calculated
471 by assuming bulk radioactive elements abundances in the silicate portion of Mercury of
472 0.2, 0.3 and 0.4 times the average surface value (the ratio between the average heat
473 production in the solid outer shell and the average surface heat production is denoted by
474 Γ; Γ = 1 implies a uniform HPE distribution in the silicate layer equivalent to the value
475 observed at the surface). *Ur* is less than 1 when F_S exceeds radioactive heat flow curves.
476 We represent the cases for (a) 4.0 Ga and (b) 3.2 Ga.
477

Table 1. Relevant parameters and surface heat flows calculated by neglecting the megaregolith layer. Surface temperature depends on both latitude and longitude due to the coupled spin-orbit resonance and the relatively high eccentricity (Vasavada et al., 1999; Williams et al., 2011).

	Lobate scarps	z_{BDT} **(km)**	T_{BDT} **(K)**	T_S **(K)**	F_S **(mW m^{-2})**
Region A	Discovery Rupes (56°S, 40°W)	35 – 40 (Watters et al., 2002)	731 - 808	365	20 - 31
Region B	Western scarp (0°, 59.3°E) Eastern scarp (0°, 64.7°E)	35 (Ritzer et al., 2010)	737 - 808	350	24 - 32
Region C	Santa Maria Rupes (3.5°N, 19°W) S_K4 scarp (4°N, 15°W) S_K3scarp (10.3°N, 13°W)	30 – 39 (Egea-Gonzalez et al., 2012)	732 - 816	435	17 - 30

Figure

Click here to download high resolution image

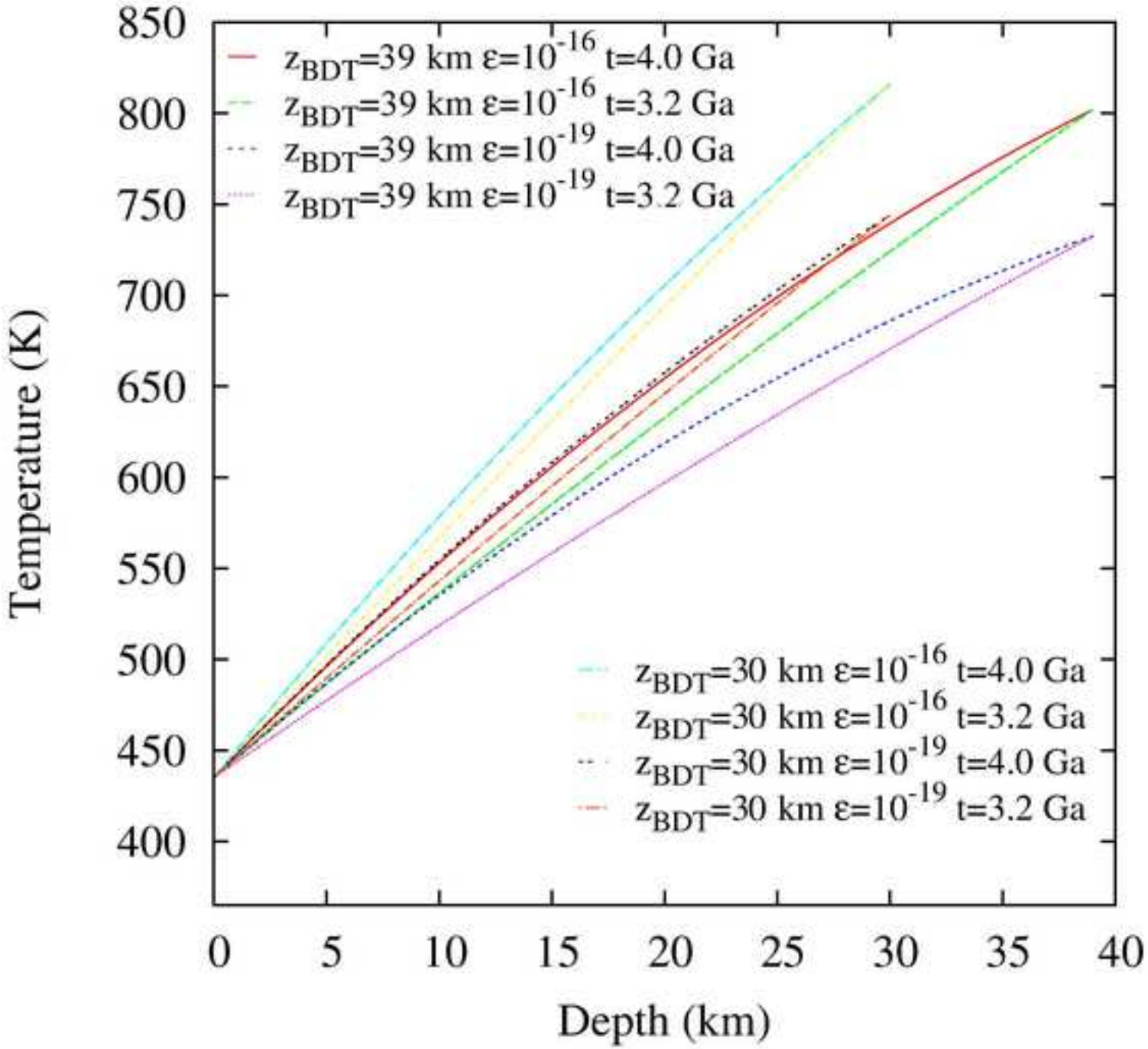

Figure
Click here to download high resolution image

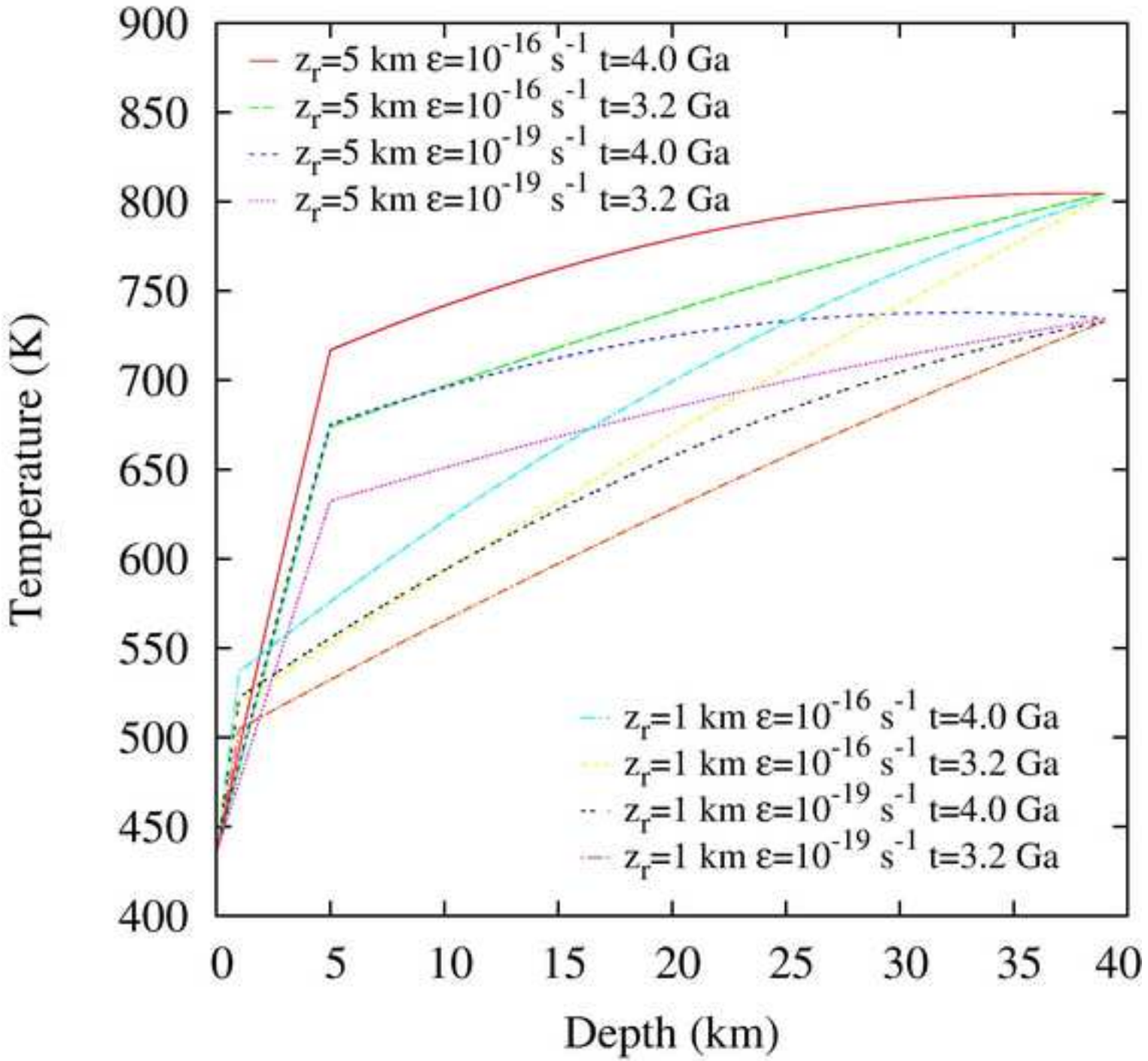

Table 2. Properties assumed in our calculations. Subscript 1 refers to the megaregolith layer and subscript 2 refers to properties of the deeper layer.

k_1 = 0.2 W m^{-1} K^{-1}	k_2 = 2.0 W m^{-1} K^{-1}
ρ_1 = 2000 kg m^{-3}	ρ_2 = 3100 kg m^{-3}
H_1 = (0.6 – 2.1) × 10^{-4} mW m^{-3} (t = 3.2 - 4.0 Ga)	H_2 = (1.0 – 3.3) × 10^{-4} mW m^{-3} (t = 3.2 - 4.0 Ga)

Table 3. Relevant parameters and extreme surface heat flows calculated by including megaregolith.

	Lobate scarps	z_{BDT} **(km)**	z_1 **(km)**	$\dot{\varepsilon}$ **(s^{-1})**	T_{BDT} **(K)**	H **($mW\ m^{-3}$)**	F_S **($mW\ m^{-2}$)**
Region A	Discovery Rupes (56°S, 40°W)	35	1	10^{-16}	808	2.1×10^{-4} 3.3×10^{-4}	25
		40	5	10^{-19}	733	0.6×10^{-4} 1.0×10^{-4}	10
Region B	Western scarp (0°, 59.3°E) Eastern scarp (0°, 64.7°E)	35	1	10^{-16}	808	2.1×10^{-4} 3.3×10^{-4}	25
			5	10^{-19}	739	0.6×10^{-4} 1.0×10^{-4}	11
Region C	Santa Maria Rupes (3.5°N, 19°W) S_K4 scarp (4°N, 15°W) S_K3 scarp (10.3°N, 13°W)	30	1	10^{-16}	816	2.1×10^{-4} 3.3×10^{-4}	23
		39	5	10^{-19}	734	0.6×10^{-4} 1.0×10^{-4}	8

Figure
Click here to download high resolution image

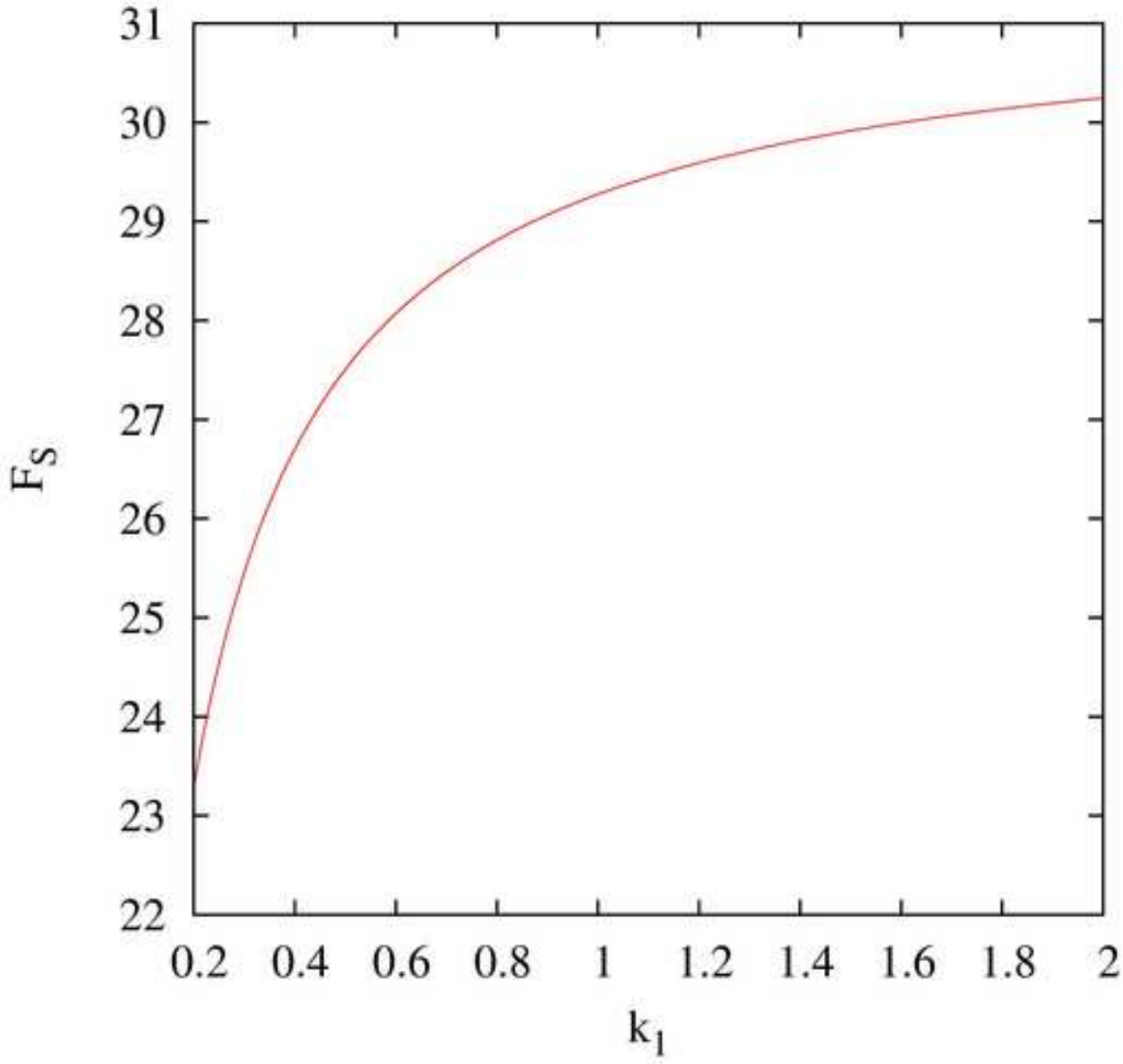

Figure
Click here to download high resolution image

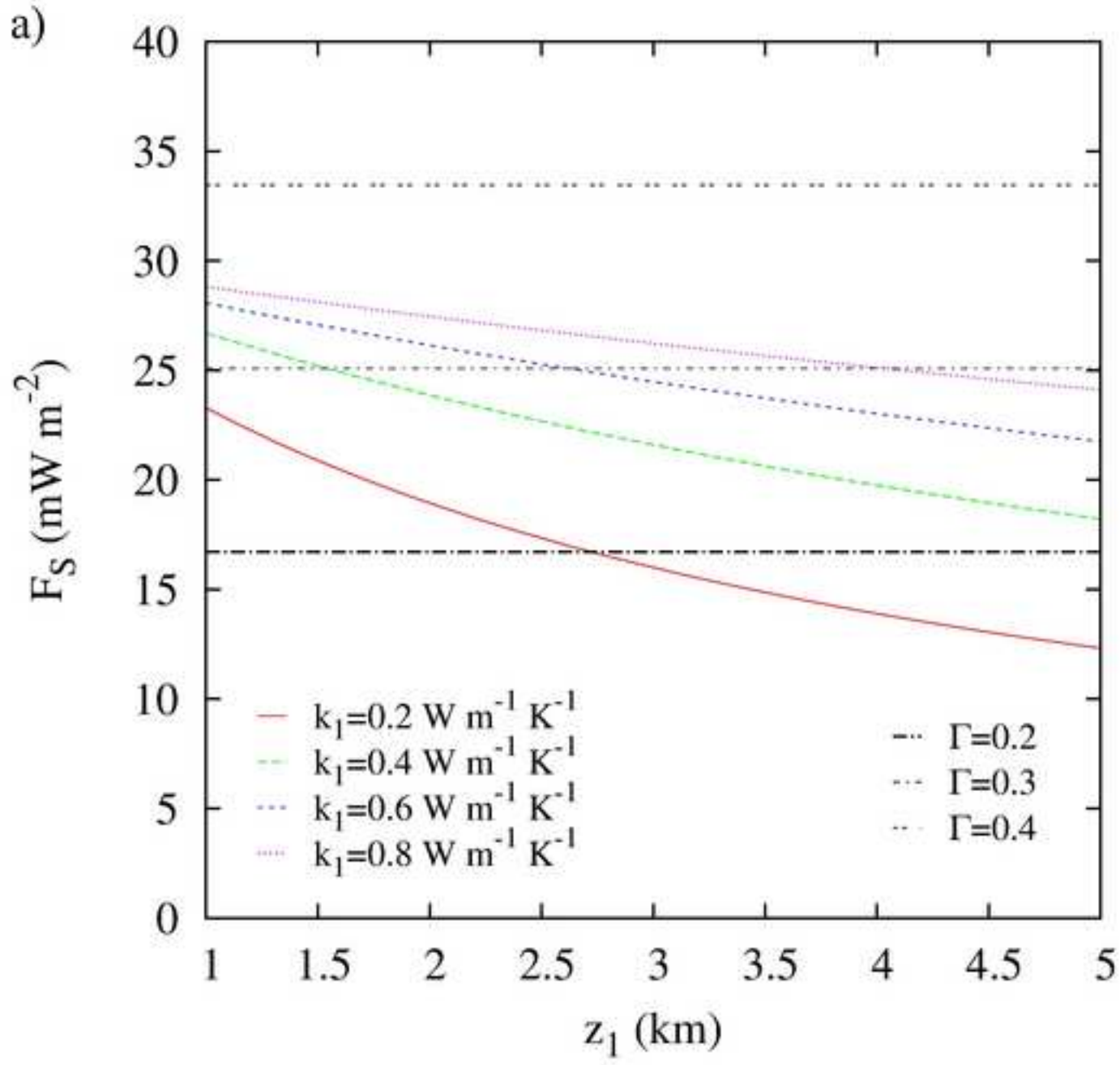

Figure
Click here to download high resolution image